Available online at www.sciencedirect.com
ScienceDirect
Journal of Magnetic Resonance 192 (2008) 92–100
JMR Journal of Magnetic Resonance
www.elsevier.com/locate/jmr

Binuclear spin state selective detection of ^{1}H single quantum transitions using triple quantum coherence: A novel method for enantiomeric discrimination

Bikash Baishya [a,b], Uday Ramesh Prabhu [a,b], N. Suryaprakash [b,*]

[a] Solid State and Structural Chemistry Unit, Indian Institute of Science, Bangalore, Karnataka 560 012, India
[b] NMR Research Centre, Indian Institute of Science, Bangalore, Karnataka 560 012, India

Received 27 November 2007; revised 29 January 2008
Available online 12 February 2008

Abstract

In the present work a novel methodology is developed for the unambiguous discrimination of enantiomers aligned in chiral liquid crystalline media and the simultaneous determination of ^{1}H–^{1}H and ^{13}C–^{1}H couplings in a single experiment. An INEPT transfer and back transfer of magnetization to protons retain the ^{13}C edited ^{1}H magnetization which is utilized to generate spin selective homonuclear triple quantum coherence of dipolar coupled methyl protons. Spin selective correlation of triple quantum to single quantum coherence results in spin state selective detection by ^{13}C spin and the remaining passive protons. The difference between the successive transitions in the triple quantum dimension pertains to sum of the passive couplings and results in enhanced resolution by a factor of three. This results in unambiguous chiral visualization. The masked ^{13}C satellite transitions in the single quantum spectrum are extracted for chiral discrimination. The technique retains all the passive homo- and heteronuclear couplings in the triple quantum dimension by the application of non-selective refocusing pulse on ^{1}H as well as on ^{13}C spins. This, however, refocuses the chemical shift evolution in the triple quantum dimension, and also overcomes the problem of field inhomogeneity. The method enables the determination of spectral information which is otherwise not possible to derive from the broad and featureless proton spectra. The elegant experimental technique has been demonstrated on different chiral molecules.

Keywords: Triple quantum NMR; Enantiomer discrimination; Chiral liquid crystal; Spectral analyses; Spin state selection; Residual dipolar couplings

1. Introduction

The NMR spectroscopic visualization of optical enantiomers is a well established tool [1,2]. However, the visualization of enantiomers using chiral derivatising agents, in the isotropic media, is not routinely feasible. The weakly aligned chiral liquid crystals, on the other hand, serves as an alternate media [3]. Unlike in thermotropic liquid crystals, the molecules in chiral liquid crystals are weakly ordered and the orientational parameters are usually in the range of 10^{-3} to 10^{-5}. The diastereomeric interaction of the *R* and *S* enantiomers with the chiral liquid crystal causes differential ordering and its effect on the order sensitive NMR spectral parameters like dipolar couplings (D_{ij}), quadrupolar couplings (Q_i) and chemical shift anisotropies ($\Delta\sigma_i$) have been exploited both for enantiomeric discrimination and to quantify their excess (ee). Due to their inherently larger strengths of interaction, the differential effect is more pronounced in quadrupole couplings than chemical shift anisotropies and dipolar couplings. Therefore, the majority of the reported work in the literature makes extensive detection of ^{2}H NMR in its natural abundance. Several one and two dimensional experiments have thus been documented for such a purpose [4–11]. Because of low gyromagnetic ratio and low natural abundance,

* Corresponding author. Fax: +91 80 2360 1550.
E-mail address: nsp@sif.iisc.ernet.in (N. Suryaprakash).

1090-7807/$ - see front matter © 2008 Elsevier Inc. All rights reserved.
doi:10.1016/j.jmr.2008.02.006

the sensitivity of ^{2}H detection is very low and hence these methods demand a large amount of the sample and enormous instrument time which may not be always feasible. While dealing with other spin $\frac{1}{2}$ nuclei like ^{13}C, the dipolar couplings and the chemical shift anisotropies are the obvious choice. As far as the employment of ^{13}C detection in its natural abundance is concerned, the possibility of detecting coupling between the dilute ^{13}C spins is one in 10^{-4} and hence the differential values of hetero-nuclear dipolar couplings and the chemical shift anisotropies have been exploited [12,13].

With high natural abundance, high magnetic moment and abundant presence in all the chiral organic molecules ^{1}H detection has significant advantages compared to other NMR active nuclei. Furthermore, it has been reported that the proton detection requires less experimental time and the errors on the quantification of enantiomeric excess is less compared to the detection of other NMR active nuclei like ^{13}C and ^{2}H [14]. Although there are exceptions, the magnitudes of $\Delta\sigma_i$ of protons are small even in strongly aligned thermotropic liquid crystals [15]. Thus the exploitation of proton $\Delta\sigma_i$ for enantiomeric discrimination is severely hampered. Nevertheless, we have reported a method using chemical shift anisotropy as an exclusive parameter for the complete unraveling of the ^{1}H NMR spectra of enantiomers by employing the homonuclear highest quantum coherence [16]. As far as the utilization of proton–proton dipolar couplings for the visualization of enantiomers is concerned, there are several experimental schemes reported in the literature [17–23].

Our attention is focused on the methodological developments to circumvent the problems and limitations in employing ^{1}H detection. Our new double quantum excited selective refocusing (DQ-SERF) method [24] results in better chiral visualization and has been demonstrated to be superior over the well known SERF experiment. Furthermore, we were able to detect long range couplings also in the direct dimension in addition to chiral discrimination in the indirect dimension. The new class of spin state selective 3Q–SQ correlation experiments, whose spin dynamics are different from that of DQ-SERF, have also been proposed by us to visualize enantiomers, simplify the complexity of ^{1}H spectra and also to determine the relative signs and magnitudes of the couplings [25]. The underlying theory of spin state selective MQ excitation as applicable to scalar coupled systems [26] and for the simplification of the spectra of dipolar coupled spins in strongly aligned media [27] have also been reported. Recently, we have also reported enantiomer visualization, complete analyses and extraction of the magnitudes and relative signs of the proton–proton couplings from the broad and featureless ^{1}H spectra by using spin selected correlation experiments [28].

In the present work, we have developed yet another methodology that exploits the natural abundant ^{13}C, as a passive spin for spin state selection. The experiment exploits the advantage of comparatively larger strengths of hetero-nuclear couplings. The ^{13}C spin state selected proton spectra provides well resolved transitions in the SQ dimension at each spin state of ^{13}C in the 3Q dimension. This resolution is further enhanced by the spin state selection of passive protons. In addition to unambiguous enantiomer discrimination, the method can be employed to extract both homo- and heteronuclear coupling information in a single experiment. The method has several distinct advantages compared to other reported methods, such as, HETSERF [20] and F_2HSQC [22]. With severe broadening of the ^{1}H spectra, it is very difficult to detect ^{13}C satellites, devoid of intense transitions from the ^{12}C attached protons and to determine ^{13}C–^{1}H couplings. The results of the study on the chiral molecules aligned in chiral liquid crystalline media are reported in this work.

2. Experimental

The oriented samples of (*R*/*S*)-3-butyn-2-ol and (*R*/*S*)-propylene carbonate whose racemic structures are given in Fig. 1, were prepared by the standard procedure described in the literature using the chiral liquid crystal poly-γ-benzyl-L-glutamate (PBLG) (DP 582) [10,21]. All the experiments were carried out on Bruker DRX 500 MHz NMR spectrometer. The one dimensional ^{1}H spectra of both the samples with expanded regions and assignments to different protons are also given in Fig. 1. The developed pulse sequence is depicted in Fig. 2. The evolution of magnetization at different stages of the pulse sequence is easily understood by the product operator formalism [29]. The pulses with rectangular shape are non-selective while the remaining pulses are spin selective. The pulse sequence of Fig. 2a starts with the non-selective INEPT transfer of magnetization from ^{1}H to ^{13}C resulting in $I_{1z}S_y$ term (where I is the proton spin and S is the ^{13}C spin) after the first 90° pulse on ^{13}C which after the second non-selective $(\pi/2)_x$ pulse on ^{13}C leads to $I_{1z}S_z$ term at point A. The INEPT transfer enables spin state selection by ^{13}C spin and also improves the overall sensitivity. This followed by a selective $(\pi/2)_x$ pulse on methyl protons leads to $I_{1y}S_z$ term at the point B, where I_{1y} corresponds to the proton magnetization of the methyl group. From the stage B to C the magnetization is allowed to evolve under the ^{1}H–^{1}H dipolar couplings among methyl protons by a selective refocusing pulse which also decouples this group from the passive protons and the ^{13}C spin. At the point C there is doubly anti phase magnetization with respect to protons, i.e., $I_{1y}I_{2z}I_{3z}S_{2z}$. The application of a selective $(\pi/2)_y$ pulse on methyl resonance converts this into $I_{1y}I_{2x}I_{3x}S_{2z}$ multiple quantum term at point D. The 3Q coherence is selected by a suitable gradient ratio and allowed to evolve under the sum of different homo- and heteronuclear passive couplings, by the non-selective refocusing pulse on ^{13}C and ^{1}H in the middle of the 3Q evolution period. This also overcomes the problem of field inhomogeneity encountered by the 3Q coherence. The last selective $(\pi/2)_x$ pulse on the methyl protons results in the observable SQ magnetization in the direct dimension.

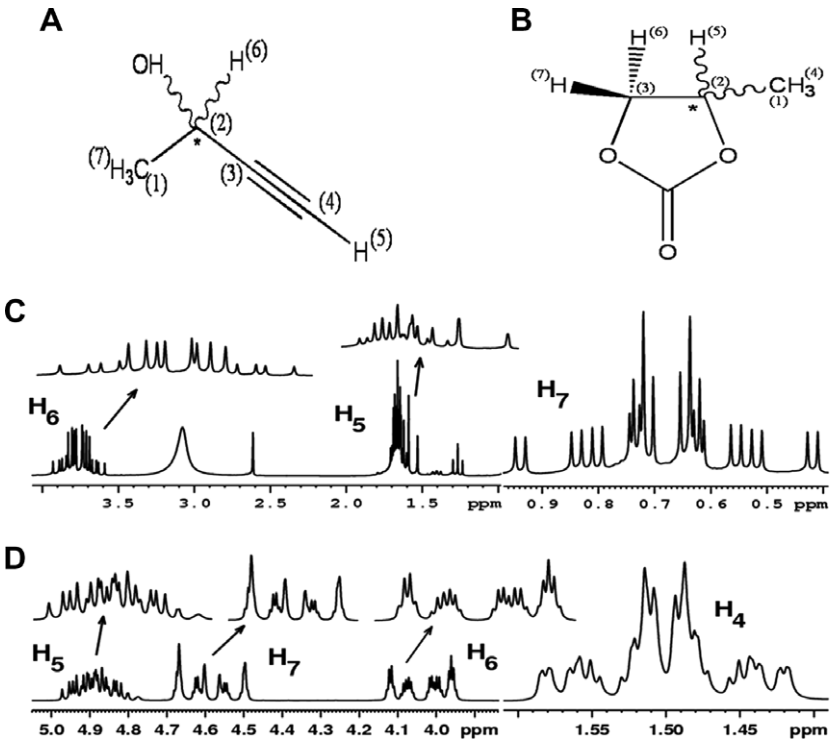

Fig. 1. The racemic structures of (A) (*R*/*S*)-3-butyn-2-ol, (B) (*R*/*S*)-propylene carbonate, (C) 500 MHz one dimensional ^{1}H spectrum of (*R*/*S*)-3-butyn-2-ol and (D) (*R*/*S*)-propylene carbonate, with expanded regions and assignments to different protons.

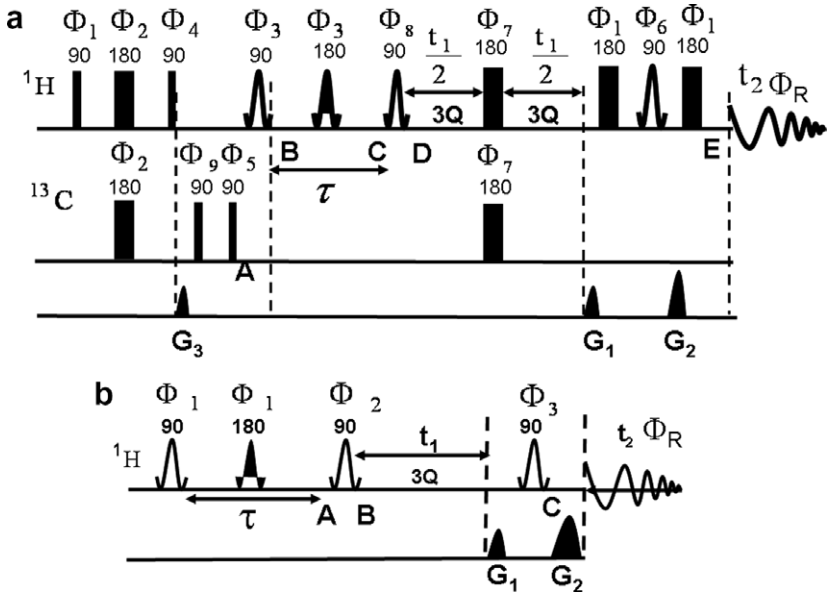

Fig. 2. The pulse sequences used for the selective excitation of ^{13}C edited 3Q–SQ coherence of methyl group in (*R*/*S*)-3-butyn-2-ol and (*R*/*S*)-propylene carbonate; (a) The pulse sequence for spin selective 3Q–SQ correlation of methyl protons edited by ^{13}C spin. The behavior of the magnetization during different stages of pulse sequences, viz. A, B, C, D and E are discussed in the text. Rectangular pulses are hard pulses. All the remaining pulses are spin selective. The phases of the pulses are; $\Phi_1 = x$, $\Phi_2 = x\,x\,x\,x\,-x\,-x\,-x\,-x$, $\Phi_3 = (12)\ x$, $\Phi_4 = y$, $\Phi_5 = x\,-x\,x\,-x\,x\,-x\,x\,-x$, $\Phi_6 = y$, $\Phi_7 = x\,x\,y\,y\,-x\,-x\,-y\,-y$, $\Phi_8 = (12)\ -y$, $\Phi_9 = x\,x\,x\,x\,x\,x\,x\,x\,-x\,-x\,-x\,-x\,-x\,-x\,-x\,-x$, $\Phi_R = x\,-x\,-x\,x\,x\,-x\,-x\,x\,-x\,x\,x\,-x\,-x\,x\,x\,-x$. (b) The pulse sequence for spin selective 3Q–SQ correlation of ^{12}C attached methyl protons. The phases of the pulses are; $\Phi_1 = (12)\ x$, $\Phi_2 = (12)\ -y$, $\Phi_3 = y$ and $\Phi_R = x$. Both the pulse sequences are not with phase sensitive detection. Hence the results of all the 2D data are represented in the magnitude mode.

The 3Q exorcycle phase cycling is used for non-selective 180° pulses in the middle of t_1 dimension. During the evolution of 3Q coherence and conversion to SQ coherence, the spin states of the remaining protons (passive spins) in the molecule and ^{13}C spin of the methyl group are undisturbed in both the dimensions. This enables the detection

of single quantum transitions of the methyl protons (A_3 spin system) based on the spin states of the passive ^1H and ^{13}C spins, which provides reduced multiplicity. In the 2D 3Q–SQ correlated spectrum, the cross-section taken along the SQ dimension for each spin state in the 3Q dimension contains individual A_3 sub spectrum and retains only the coupling among the active spins. This dramatically simplifies the analysis compared to analyzing the large number of crowded and unresolved transitions of a one dimensional ^1H spectrum arising from the overlap of all the sub spectra. Furthermore, there is a displacement of different sub spectra in the SQ cross-sections for different spin states of the binuclear spins analogous to the E-COSY experiment [30,31], which depends on the magnitudes of the passive couplings.

In (*R*/*S*)-3-butyn-2-ol all the resonances are well isolated and the methyl protons of both the enantiomers could be selectively excited, as the anisotropic chemical shift difference between the methyl peaks for two enantiomers are negligible. The optimization of the τ delay between the first and the second selective $\pi/2$ pulse on methyl protons is very important in view of the differential dipolar couplings among the methyl protons in each enantiomer. A series of experiments were, therefore, carried out to optimize the τ delay for getting the maximum signal intensity for the methyl group. The intensity of the first row of the 3Q–SQ spectrum corresponding to each enantiomer was plotted as a function of τ delay. The delay which gave maximum and comparable intensities for both the enantiomers was taken and reported in the figure caption. The similar procedure was followed for (*R*/*S*)-propylene carbonate to optimize the τ delay. The extensive discussion on the optimization of τ delay has already been reported in our earlier work [24]. All the acquisition and processing parameters for each experiment is reported in the corresponding figure captions. During processing linear prediction was also attempted to obtain spectra with undistorted base line. All the spectra are reported in the magnitude mode.

3. Results and discussion

3.1. The analyses of the spectra of (*R*/*S*)-3-butyn-2-ol

The one dimensional ^1H spectrum of (*R*/*S*)-3-butyn-2-ol in the chiral liquid crystal PBLG has well isolated peaks for all the group of protons. Considering the one percent molecule where the protons of the methyl group are attached to ^{13}C, the spin system is of the type A_3MPX, where A refers to methyl protons, M and P corresponds to methine and acetylenic protons and X is the ^{13}C spin. The first order analysis of the spectrum is straightforward. The methyl protons are split into 1:2:1 triplet due to residual dipolar couplings among them. The separation between the two adjacent transitions provides $^2T_{HH}$ ($3D_{HH}$) where the superscript 2 refers to protons that are two bonds away. Each of these transitions is further split into doublet of a doublet of equal intensity due to couplings from methine and acetylenic protons. The number of transitions is doubled by the hetero-nuclear coupling which results in the satellite spectra. Thus the 24 theoretically allowed transitions of methyl protons from each enantiomer can be construed as eight sub spectra according to eight possible spin states of M, P and X spins. In the developed pulse sequence we separate all the eight sub spectra from each other, and detect them independently in well separated arrays of SQ dimension. Similarly, the splitting pattern of methine and acetylenic groups can be interpreted using first order analyses. The assignments to *R* and *S* enantiomers are taken from the literature [3]. The anisotropic proton chemical shift difference between the two enantiomers is negligibly small and hence the two sets of peaks arising from both *R* and *S* enantiomers are overlapped for the ^{12}C bound 1D ^1H spectra as well as the ^{13}C bound satellite proton spectra.

The pulse scheme shown in Fig. 2a leads to spin selective 3Q–SQ correlation of ^{13}C attached methyl protons. The selectively methyl protons excited 2D 3Q–SQ spectrum is shown in Fig. 3 along with F_1 and F_2 projections. The intensity of the peaks given in the projections might not agree with those predicted by the first order analyses. This is also because the optimized τ delay will not result in uniform coherence transfer. However, one should keep in mind, F_2 projections pertain to the satellite spectra and the polarization transfer to different types of carbons during the INEPT sequence may also not be uniform. The detailed discussion on the intensity during the HSQC sequence for molecules aligned in thermotropic liquid crystals has been reported by us recently [32]. The selective excitation of 3Q coherence of the methyl protons results in the simultaneous flipping of all the protons. However, the non-selective refocusing pulse on ^{13}C and ^1H leads to refocusing of chemical shift evolution and retain the hetero-nuclear and different passive homonuclear couplings in the 3Q dimension. Thus the spin system in the 3Q dimension will be of the type AMPX, where A is the super spin with three methyl protons. The 3Q dimension will be the A part of this AMPX type spin system. The F_2 projection is the ^{13}C satellite proton spectrum with maximum suppression of peaks from ^{12}C attached protons. The connectivity of 3Q–SQ direct peaks form a distinct pattern for each enantiomer in the 2D spectrum which unambiguously discriminate the enantiomers.

In the 3Q dimension, the largest coupling to A spin is from the $J_{CH} + 2D_{CH}$, where J_{CH} and D_{CH} are the scalar and the dipolar couplings between protons and ^{13}C of the methyl group. In the spin product basis set the 3Q states of proton are $|\alpha_A\alpha_A\alpha_A>$ and $|\beta_A\beta_A\beta_A>$. This is coupled to spin states $|\alpha>$ and $|\beta>$ of ^{13}C spin. Hence the resonance of spin A is split into a doublet. Two such doublets are expected in the 3Q dimension corresponding to one for each enantiomer. The value of D_{CH} being different for both the enantiomers and the scaling of the ($J_{CH} + 2D_{CH}$) by a

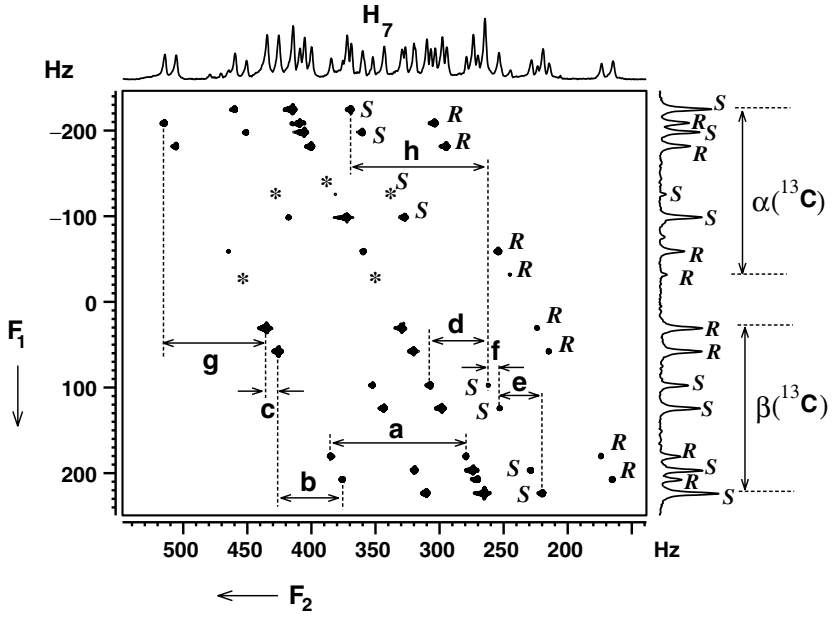

Fig. 3. Selective methyl protons excited 2D 3Q–SQ correlated spectrum of (*R*/*S*)-3-butyn-2-ol along with the corresponding projections. The optimized τ delay is 10 ms. The seduced shape pulse lengths are 4.16 and 6.9 ms for 90° and 180° selective pulses, respectively, with rf power optimized accordingly. The 2D data matrix is 1.3 k and 384 points in F_2 (SQ) and F_1 (3Q) dimensions, respectively. Spectral widths of 600 and 500 Hz were chosen in the direct and indirect dimensions, respectively. The number of accumulations was 16 for each t_1 increment. Relaxation delay used was 4 s. The time domain data was processed by zero filling it to 2 k and 1 k points in F_2 and F_1 dimensions, respectively, with sine square bell window function and with linear prediction to 512 points, to obtain high resolution and undistorted baseline, in the F_1 dimension. The spectrum was displayed in magnitude mode with a digital resolution of 0.29 and 0.48 Hz in the direct and indirect dimensions, respectively. F_1 dimension pertains to 3Q spectrum. $\alpha(^{13}C)$ and $\beta(^{13}C)$ regions are marked in the F_1 dimension. The total experimental time is around 7 h. The assignments to *R* and *S* transitions are marked. The separations marked with alphabets, a to h providing coupling parameters are discussed in the text and reported in the Table 1. The * marks represent transitions of low intensities.

factor of three, due to magnetic equivalence, resulted in enhanced spectral resolution and unambiguous enantiomer visualization. This also can be construed as the separation of ^{13}C satellites in the one dimensional spectrum with suppression of transitions from ^{12}C attached protons. From the doublet separations for each enantiomer the values i.e., $^1T_{CH}\ (3T^R) = (3(J_{CH} + 2D_{CH})^R)$ and $^1T_{CH}\ (3T^S) = (3(J_{CH} + 2D_{CH})^S)$ could be determined as 432.0 and 409.2 Hz, respectively.

The two 3Q transitions edited by the ^{13}C spin states are further split by the remaining two methine and acetylenic protons into four transitions according to their four spin states $|\alpha_M\alpha_P>$, $|\alpha_M\beta_P>$, $|\beta_M\alpha_P>$ and $|\beta_M\beta_P>$. Thus a total of eight 3Q transitions are observed for each enantiomer. One set of four transitions correspond to $|\alpha>$ state of ^{13}C while the other set of four transitions correspond to $|\beta>$ state. The 3Q transitions corresponding to $|\alpha>$ and $|\beta>$ domains of ^{13}C are marked as $\alpha(^{13}C)$ and $\beta(^{13}C)$ in Fig. 3. Chiral discrimination is obvious from the highly resolved 3Q spectrum in the F_1 dimension. Such high resolution is not possible to obtain from the one dimensional ^1H spectra with or without ^{13}C satellites. The sub spectral analyses at any one of the ^{13}C spin states provides the coupling of methyl protons to all the passive protons. The different displacement vectors *g* and *h*, *b* and *e*, *c* and *f* between sub spectra drawn in Fig. 3 provides passive coupling parameters $J_{CH} + 2D_{CH}$, $^3T_{HH}$ and $^5T_{HH}$ for the enantiomers. The derived spectral parameters are reported in Table 1.

The cross-sections taken along the SQ dimension at different passive proton spin states of 3Q dimension for the $\beta(^{13}C)$ region is plotted in Fig. 4a–h. Each of these cross-sections pertains to selectively detected SQ transitions originating from the 3Q transition whose initial and final states have the same passive spin state. An example of such a SQ transition is from the state $|\alpha_A\alpha_A\alpha_A\beta_M\beta_P\beta_X>$ to $|\beta_A\alpha_A\alpha_A\beta_M\beta_P\beta_X>$ which arises from a 3Q transition like $|\alpha_A\alpha_A\alpha_A\beta_M\beta_P\beta_X>$ to $|\beta_A\beta_A\beta_A\beta_M\beta_P\beta_X>$ where the initial and final passive spin state is $|\beta_M\beta_P\beta_X>$. A theoretical description of this is available in our recently reported work [26]. Thus all the proton SQ transitions pertaining to eight A_3 sub spectra get separated into different cross-sections depending on the spin states of the passive spins. The Eigen values of $M_Z(=\Sigma I_Z$ (M, P, X)) are to be considered as good quantum numbers and as a special rule for allowed A_3 transitions in each cross section it follows that $\Delta M_Z = 0$. Also each cross-section is a triplet, from which D_{HH} among methyl protons can be determined. Thus 'a' and 'd' marked in Fig. 3 provides $^2T_{HH}$ of *R* and *S* enantiomers, respectively. It may be pointed out that in a non-selective MQ–SQ correlation experiment it is not possible to separate sub spectra into different cross-sections and hence the dramatic resolution cannot be achieved unlike in the present scheme. Looking into the individual sub

Table 1
The derived coupling parameters (only magnitudes have been determined and not the signs of the couplings) from the 3Q–SQ correlation experiments in (*R*/*S*)-3-butyn-2-ol and (*R*/*S*)-propylene carbonate

(*R*/*S*)-3-butyn-2-ol			(*R*/*S*)-propylene carbonate		
Parameter	Designation in the figure caption	Value in Hz	Parameter	Designation in the figure caption	Value in Hz
$(3\times{}^2D_{H7H7})^S$	d	45.4	$(3\times{}^2D_{H4H4})^S$	b	18.3
$({}^3T_{H6H7})^S$	e	33.0	$({}^3T_{H4H5})^S$	c	13.7
$({}^5T_{H5H7})^S$	f	8.9	$({}^4T_{H4H6})^S$	d	3.3
$({}^1T_{C1H7})^S$	h	107.7	$({}^4T_{H4H7})^S$	e	3.3
$(3\times{}^2D_{H7H7})^R$	a	105.4	$({}^1T_{C1H4})^S$	a	136.4
$({}^3T_{H6H7})^R$	b	50.0	$(3\times{}^2D_{H4H4})^R$	g	35.6
$({}^5T_{H5H7})^R$	c	9.0	$({}^3T_{H4H5})^R$	h	9.3
$({}^1T_{C1H7})^R$	g	79.8	$({}^4T_{H4H6})^R$	i	3.0
			$({}^4T_{H4H7})^R$	j	0.9
			$({}^1T_{C1H4})^R$	f	144.0

The errors on the reported couplings are governed by the digital resolution reported in the figure captions. For the precision of the parameters, to be on the safer side, the errors can be taken as 2 or 3 times the digital resolution.

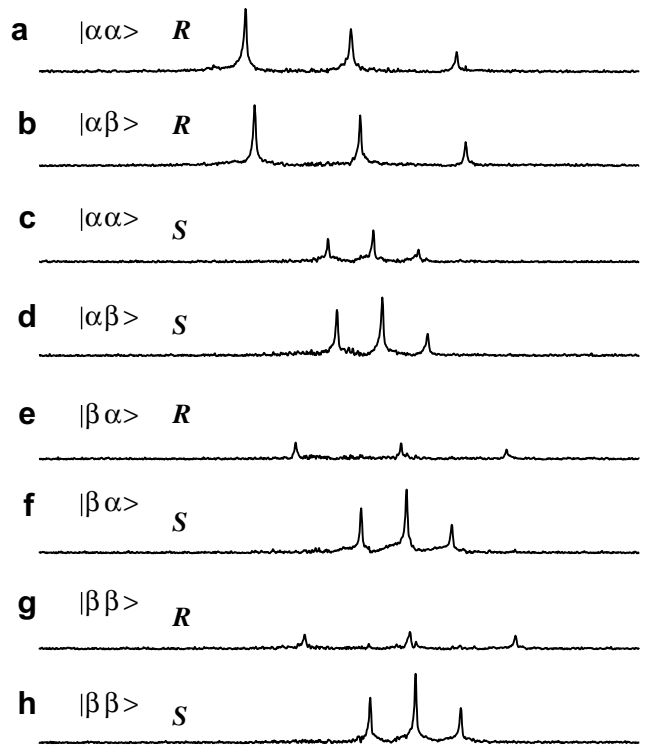

Fig. 4. (a–h) The cross-sections taken along F_2 dimension for each sub spectrum edited by passive spin states in Fig. 3, plotted with same horizontal scale for comparison. Only the cross-sections pertaining to $\beta({}^{13}C)$ regions are given. *R* and *S* assignments and the passive proton spin states in the 3Q dimension are shown.

spectrum and a distinct connectivity of the transitions in the 2D plane makes discrimination and analyses simpler.

A comparison of the 3Q–SQ correlation for ^{12}C attached protons and ^{13}C attached protons is shown in Fig. 5. The $\beta({}^{13}C)$ region is plotted separately in the expanded scale for comparison. The 3Q–SQ correlation of ^{12}C attached protons leads to spin state selection by only passive proton spins and discriminate 20 out of 24 transitions. The transitions marked with star represent the overlap of two transitions from the two enantiomers. The 3Q–SQ correlation of ^{13}C attached protons discriminate all the 24 transitions, a consequence of further spin state selection by the ^{13}C spin.

3.2. The analyses of the spectra of (*R*/*S*)-propylene carbonate

To ascertain the robustness of the developed methodology, the technique was applied to another molecule, (*R*/*S*)-propylene carbonate. The protons and carbon of the methyl group of this molecule form a weakly coupled spin system of the type A_3MNPX where A_3 corresponds to active methyl protons, M and N are the two methylene protons, P is the methine proton and X is the ^{13}C spin. The methyl protons experience five different type of couplings, viz. (a) the couplings among themselves ($^2T_{HH}$) leading to a triplet, (b) the coupling between methyl and methine (P) protons ($^3T_{HH}$) giving a doublet for each transition of the triplet, (c) the two different couplings from the two diastereomeric methylene protons (M and N, protons numbered 6 and 7 in Fig. 1B) giving rise to further splitting of each transition to doublet of doublet ($^4T_{HH}$) and (d) the coupling from the ^{13}C spin (X) leading to a larger doublet owing to hetero-nuclear coupling. The 48 transitions observed for each enantiomer can be visualized as 16 A_3 sub spectra corresponding to 16 passive spin states of M, N, P and X together. Thus there are total of 96 overlapped transitions from both the enantiomers. Furthermore, there will also be an overlap of transitions from the protons attached to ^{12}C. It is evident from the methyl region of the spectrum (Fig. 1D) that resolving these many transitions to obtain spectral parameters is a challenging task.

The selective methyl protons excited two dimensional 3Q–SQ correlated spectrum of (*R*/*S*)-propylene carbonate is given in Fig. 6. In the 3Q dimension, the spin system is of the type AMNPX. The super spin A is the three methyl protons (the active spin), the methine and methylene protons (M, N and P) and one ^{13}C spin (X) constitute the passive spins. $^2T_{HH}$ in A_3 is the active coupling while one

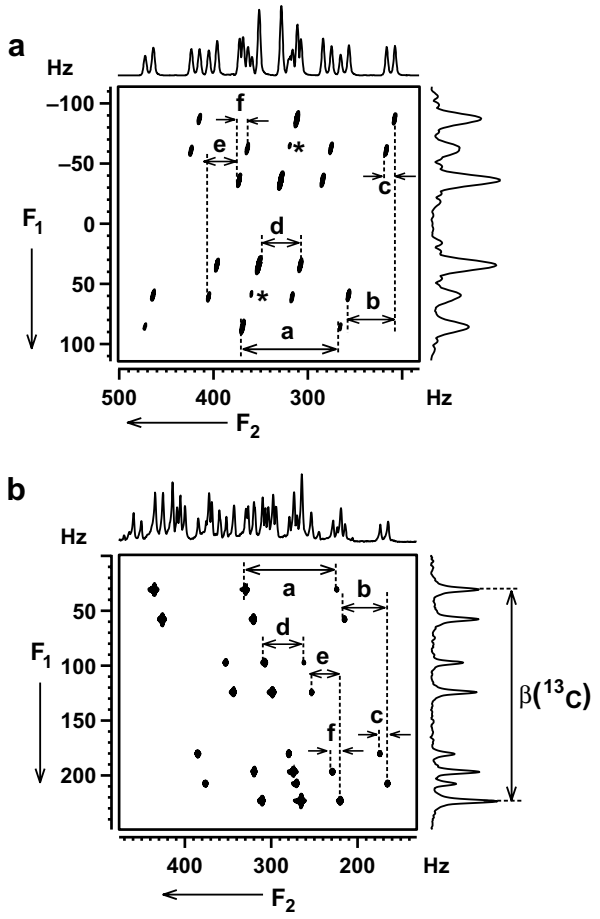

Fig. 5. (a) ^{12}C attached methyl protons excited 2D 3Q–SQ correlated spectrum of (*R*/*S*)-3-butyn-2-ol obtained using pulse sequence 2b, along with the corresponding projections. The 2D data matrix is 1228 × 336 and zero filled to 4 k and 1 k before processing. The sine bell window function is used in both the dimensions. Four scans for each FID and a recycle delay of 7 s. The optimized τ delay is 10 ms. The seduce shaped pulse lengths are 6.25 ms for both 90° and 180° pulses with different power levels. Digital resolution is 0.5 and 0.1 Hz in F_1 and F_2 dimensions. Assignments of spin state selected sub spectrum to *R* and *S* enantiomers are shown. * marks indicate the overlap of two transitions from *R* and *S*. The separations a, b and c marked provide $^2T_{HH}$, $^3T_{HH}$ and $^5T_{HH}$ for *R* enantiomer and those marked with d, e and f provide the similar information for *S* enantiomer. (b) ^{13}C edited methyl protons excited 2D 3Q–SQ correlated spectrum of (*R*/*S*)-3-butyn-2-ol along with the corresponding projections using pulse sequence 2a shown in Fig. 3. Only $\beta(^{13}C)$ region is plotted in expanded scale. Assignments of spin state selected sub spectrum to *R* and *S* enantiomers are shown. Note the advantage of spin state selection in the discrimination of even the peaks marked with * of Fig. 4a. Separations providing coupling information are marked in Fig. 3.

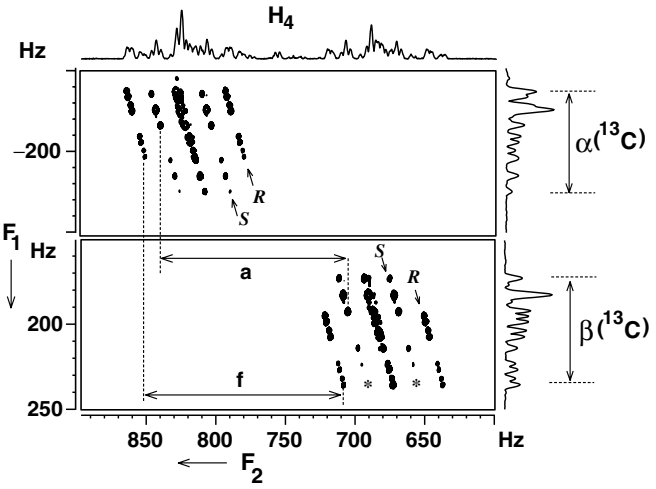

Fig. 6. Methyl protons excited 2D 3Q–SQ correlated spectrum of (*R*/*S*)-propylene carbonate along with the corresponding projections. The optimized τ delay is 25 ms. The seduced shape pulse lengths are 3.125 and 3.7 ms for 90° and 180° pulses, respectively. The 2D data matrix of 800 and 576 points in F_2 (SQ) and F_1 (triple quantum) dimensions, respectively, were chosen. Spectral widths of 535 and 300 Hz were chosen in the direct and indirect dimensions, respectively. The number of accumulations was 24 for each t_1 increment. Relaxation delay used was 3 s. The time domain data was processed by zero filling it to 2 and 1 k points in F_2 and F_1 dimensions, respectively, with sine bell window function and without linear prediction. The spectrum was displayed in magnitude mode with digital resolutions of 0.15 and 0.52 Hz in the direct and indirect dimensions, respectively. F_1 dimension pertains to 3Q spectrum. $\alpha(^{13}C)$ and $\beta(^{13}C)$ regions are marked in the F_1 dimension. The assignment of peaks to *R* and *S* marked and also shown with tilted arrows. The displacements of $\alpha(^{13}C)$ and $\beta(^{13}C)$ regions in the F_2 dimension providing hetero-nuclear passive couplings are marked as a and f for *S* and *R* enantiomers, respectively. These values are reported in Table 1. Peaks with very low intensities are marked with *.

$^3T_{HH}$ and two $^4T_{HH}$ along with hetero-nuclear $^1T_{CH}$ constitute the passive couplings. The 3Q dimension provides 16 transitions for each enantiomer pertaining to 16 spin states of M, N, P and X. The displacements between the SQ transitions corresponding to $|\alpha>$ and $\beta>$ domains of ^{13}C marked 'a' and 'f' in Fig. 6 are equal to the size of the passive hetero-nuclear coupling $^1T_{CH}$ for the *S* and *R* enantiomers, respectively.

It can be observed from the Fig. 6 that the analyses of the spectra at any one of the spin states of ^{13}C is sufficient to derive all the homonuclear couplings involved with methyl protons. The assignment of peaks to *R* and *S* enantiomers is taken from the literature [18]. Analysis of the expanded spectral region corresponding to $|\alpha>$ spin state of ^{13}C displayed in Fig. 7 was carried out. For the *S* enantiomer the two types of $^4T_{HH}$ are equal and hence results in a triplet of a doublet (due to $^3T_{HH}$) in the 3Q dimension and are marked *S* in Fig. 7. However, for the *R* enantiomer the two types of $^4T_{HH}$ are unequal. Hence 3Q dimension provides eight distinct transitions marked *R* in the figure.

Alphabets marked 'b' and 'g' in Fig. 7 denote the active coupling $^2T_{HH}$ responsible for the triplet (sub spectrum) in each SQ cross-section for the *S* and *R* enantiomers, respectively. Thus each cross-section taken along the SQ dimension for each passive spin state in 3Q dimension is a triplet. The eight A_3 sub spectra (triplets) for eight passive spin states are observed for *R* enantiomer. However, for *S* enantiomer, six triplets with smaller dipolar couplings are observed. The passive homonuclear couplings are determined from the displacements marked c, d, e and h, i, j for the *S* and *R* enantiomers, respectively. We are very much aware that the coupling information among protons numbered, 5, 6 and 7 are not reflected either in the 3Q or in the SQ dimension. However, the selective excitation of

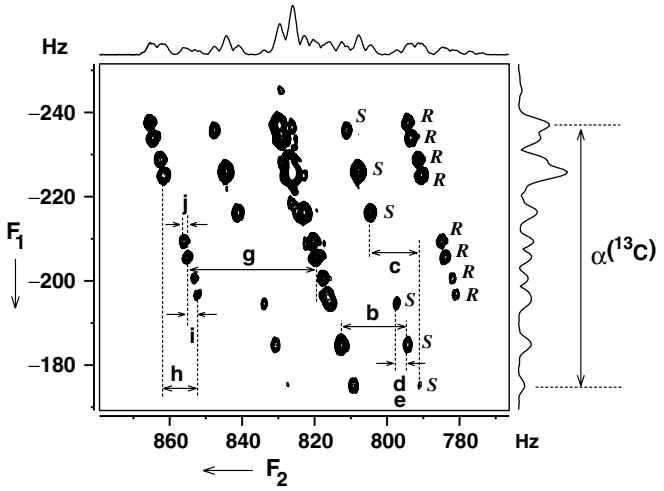

Fig. 7. The expanded $\alpha(^{13}C)$ region of Fig. 6. The separations marked with alphabets b–e and g–j provide proton–proton coupling information and the corresponding values are reported in Table 1. Assignments to the enantiomer peaks are marked.

these protons edited by their respective ^{13}C spins provides the totality of the coupling information. All the proton–proton couplings for these molecules have been reported in our earlier works [25,28]. The aim of our present study is to demonstrate the experimental methodology. Hence only the few couplings determined in this study are reported in Table 1.

3.3. The advantages and limitations of the present method

The present study has numerous advantages, viz.,

(a) Separation of complex 1D spectrum into the component sub spectra. The resolution in the individual sub spectra is dramatic. This leads to better and unambiguous enantiomeric discrimination. This is significant compared to DQ-SERF experiment.
(b) It is possible to determine both homo- and hetero-nuclear couplings in a single experiment.
(c) The masked ^{13}C satellites in single quantum spectrum are completely separated, devoid of peaks from protons attached to ^{12}C carbons and utilized for chiral discrimination.
(d) Active and passive couplings are separated in two dimensions leading to spectral simplification rendering the easy analysis of the first order spectra. This is not possible either in the 1D spectrum or in the DQ-SERF experiment reported earlier.
(e) Implementing ^{13}C spin state selection in addition to ^{1}H spin state leads to further improvement in discrimination as demonstrated in Fig. 5.
(f) The measured parameters are precise due to upward scaling of the couplings.

The method also suffers from certain limitations. The technique cannot be applied to strongly coupled spins as the selective excitation is not possible. The MQ excitation being non-uniform [33], the quantification of enantiomeric excess is tedious.

In general, the technique is applicable to any molecule. However, the requirement is at least one group of protons should be isolated for the selective excitation of higher quantum. The study on different complicated systems to detect higher order coherence to achieve spin state selection, for enantiomer discrimination and to determine all the coupling information is in progress and will be published elsewhere.

4. Conclusions

The present study employs chiral liquid crystal for enantiomeric discrimination using natural abundant ^{13}C as a passive spin for the state selective 3Q–SQ correlation. There are significant advantages of such a study. Complex spectrum is split into highly resolved sub spectra and active and passive couplings are separated from each other. The passive coupling information is available from 3Q dimension as well as from the displacements in the SQ dimension. Both 3Q as well as SQ spectra are utilized for the chiral discrimination. The 3Q dimension provides three times enhancement in resolution. Because of the spin state selective detection of SQ transitions the sub spectra are separated from each other which further enhance the resolution in the SQ dimension. Consequently, the problem of overlap of two enantiomer spectra has been overcome. A comparison of 3Q –SQ correlation for 3-butyn-2-ol for ^{12}C as well as ^{13}C attached protons demonstrates the advantage of ^{13}C spin state selection. The hetero-nuclear coupling for the methyl group is also available from the spectrum. Active coupling among methyl protons are determined from the SQ cross-sections. The determination of spectral parameters is significantly simplified. The larger dispersion of the spectrum aided the better discrimination of enantiomers.

Acknowledgments

NS gratefully acknowledges the financial support by Department of Science and Technology, New Delhi for the Grant No. SR/S1/PC-13/2004. BB and URP thanks Council of Scientific and Industrial Research (CSIR), India for the research fellowship.

References

[1] D. Parker, NMR determination of enantiomeric purity, Chem. Rev. 91 (1991) 1441–1457.
[2] R. Rothchild, NMR methods for determination of enantiomeric excess, Enantiomer 5 (2000) 457–471.
[3] P. Lesot, D. Merlet, J. Courtieu, J.W. Emsley, T.T. Rantala, J. Jokisaari, Calculation of the molecular ordering parameters of (±)-3-butyn-2-ol dissolved in organic solutions of poly-γ-benzyl-L-glutamate, J. Phys. Chem. A. 101 (1997) 5719–5724.

[4] O. Lafon, P. Lesot, D. Merlet, J. Courtieu, Modified z-gradient filtering as a mean to obtain phased deuterium auto correlation 2D NMR spectra in oriented solvents, J. Magn. Reson. 171 (2004) 135–142.
[5] I. Canet, J. Courtieu, A. Loewenstein, A. Meddour, J.M. Péchiné, Enantiomeric analysis in polypeptide lyotropic liquid crystal by deuterium NMR, J. Am. Chem. Soc. 117 (1995) 6520–6526.
[6] I. Canet, A. Meddour, J. Courtieu, New, and accurate method to determine the enantiomeric purity of amino acids based on deuterium NMR in a cholesteric lyotropic liquid crystal, J. Am. Chem. Soc. 116 (1994) 2155–2156.
[7] D. Merlet, M. Sarfati, B. Ancian, J. Courtieu, P. Lesot, Description of natural abundance deuterium 2D NMR experiments in weakly ordered liquid-crystalline solvents using a tailored Cartesian spin-operator formalism, Phys. Chem. Chem. Phys. 2 (2000) 2283–2290.
[8] P. Lesot, D. Merlet, A. Loewenstein, J. Courtieu, Enantiomeric visualisation using proton-decoupled natural abundance deuterium NMR in poly(γ-benzyl-L-glutamate) liquid crystalline solutions, Tetrahedron Asymm. 9 (1998) 1871–1881.
[9] D. Merlet, B. Ancian, W. Smadja, J. Courtieu, P. Lesot, Analysis of natural abundance deuterium NMR spectra of enantiomers in chiral liquid crystals *via* 2D auto-correlation experiments, Chem. Commun. (1998) 2301–2302.
[10] D. Merlet, B. Ancian, J. Courtieu, P. Lesot, Two-dimensional deuterium NMR spectroscopy of chiral molecules oriented in a polypeptide liquid crystal: applications for the enantiomeric analysis through natural abundance deuterium NMR, J. Am. Chem. Soc. 121 (1999) 5249–5258.
[11] I. Canet, J. Lovschall, J. Courtieu, Visualization of enantiomers through deuterium NMR in cholesterics. Optimization of the chiral liquid crystal solvent, Liq. Cryst. 16 (1994) 405–412.
[12] P. Lesot, O. Lafon, J. Courtieu, P. Berdagué, Analysis of the ^{13}C NMR spectra of molecules, chiral by isotopic substitution, dissolved in a chiral oriented environment: towards the absolute assignment of the pro-R/pro-S character of enantiotopic ligands in prochiral molecules, Chem. Eur. J. 10 (2004) 3741–3746.
[13] A. Meddour, P. Berdague, A. Hedli, J. Courtieu, P. Lesot, Proton-decoupled carbon-13 NMR spectroscopy in a lyotropic chiral nematic solvent as an analytical tool for the measurement of the enantiomeric excess, J. Am. Chem. Soc. 119 (1997) 4502–4508.
[14] M. Sarfati, P. Lesot, D. Merlet, J. Courtieu, Theoretical and experimental aspects of enantiomeric differentiation using natural abundance multinuclear NMR spectroscopy in chiral polypeptide liquid crystals, Chem. Commun. (2000) 2069–2081.
[15] J. Lounila, J. Jokisaari, Anisotropies in spin–spin coupling constants and chemical shifts as determined from the NMR spectra of molecules oriented by liquid crystal solvents, Prog. NMR Spectrosc. 15 (1982) 249–290.
[16] R.P. Uday, B. Bikash, N. Suryaprakash, Chemical shift anisotropy edited complete unraveling of overlapped ^{1}H NMR spectra of enantiomers: application to small chiral molecules, J. Magn. Reson. 191 (2008) 259–266.
[17] J. Farjon, D. Merlet, P. Lesot, J. Courtieu, Enantiomeric excess measurements in weakly oriented chiral liquid crystal solvents through 2D ^{1}H selective refocusing experiments, J. Magn. Reson. 158 (2002) 169–172.
[18] L. Beguin, J. Courtieu, L. Ziani, D. Merlet, Simplification of the ^{1}H NMR spectra of enantiomers dissolved in chiral liquid crystals, combining variable angle sample spinning and selective refocusing experiments, Magn. Reson. Chem. 44 (2006) 1096–1101.
[19] P. Lesot, D. Merlet, J. Courtieu, J.W. Emsley, Discrimination and analysis of the NMR Spectra of enantiomers dissolved in chiral liquid crystal solvents through 2D correlation experiments, Liq. Cryst. 21 (1996) 427–435.
[20] J. Farjon, J.P. Baltaze, P. Lesot, D. Merlet, J. Courtieu, Heteronuclear selective refocusing 2D NMR experiments for the spectral analysis of enantiomers in chiral oriented solvents, Magn. Reson. Chem. 42 (2004) 594–599.
[21] L. Ziani, J. Courtieu, D. Merlet, Visualisation of enantiomers via insertion of a BIRD module in X–H correlation experiments in chiral liquid crystal solvent, J. Magn. Reson. 183 (2006) 60–67.
[22] V.M. Marathias, I. Goljer, A.C. Bach II, Simultaneous determination of ^{1}H–^{1}H and ^{1}H–^{13}C residual dipolar couplings in a chiral liquid crystal solvent using a natural abundance HSQC experiment, Magn. Reson. Chem. 43 (2005) 512–519.
[23] V.M. Marathias, G.J. Tawa, I. Goljer, A.C. Bach II, Sterochemical identification of (*R*)- and (*S*)-Ibuprofen using residual dipolar couplings, NMR, Modeling, Chirality 19 (2007) 741–750.
[24] B. Bikash, R.P. Uday, N. Suryaprakash, Enantiomeric discrimination by double quantum excited selective refocusing (DQ-SERF) experiment, J. Phys. Chem. B. 111 (2007) 12403–12410.
[25] B. Bikash, R.P. Uday, N. Suryaprakash, Chiral discrimination and the complete analyses of the overlapped and unresolved ^{1}H NMR spectra of enantiomers by multiple quantum spin state selection, J. Magn. Reson., submitted for publication.
[26] B. Bikash, N. Suryaprkash, Spin selective multiple quantum NMR for spectral simplification, determination of relative signs and magnitudes of scalar couplings by spin state selection, J. Chem. Phys 127 (2007) 214510.
[27] B. Bikash, N. Suryaprakash, Spin state selective detection of single quantum transitions using multiple quantum coherence: simplifying the analyses of complex NMR spectra, J. Phys. Chem. A. 111 (2007) 5211–5217.
[28] R.P. Uday, B. Bikash, N. Suryaprakash, Separation and complete analyses of the overlapped and unresolved ^{1}H NMR spectra of enantiomers by spin selected correlation experiments, J. Phys. Chem., submitted for publication.
[29] O.W. Sørensen, G.W. Eich, M.H. Levitt, G. Bodenhausen, R.R. Ernst, Product operator formalism for the description of NMR pulse experiments, Prog. NMR Spectrosc. 16 (1983) 163–192.
[30] C. Griesinger, O.W. Sørensen, R.R. Ernst, Two-dimensional correlation of connected NMR transitions, J. Am. Chem. Soc. 107 (1985) 6394–6396.
[31] C. Griesinger, O.W. Sørensen, R.R. Ernst, Correlation of connected transitions by two-dimensional NMR spectroscopy, J. Chem. Phys. 85 (1986) 6837–6852.
[32] B. Bikash, R.G. Mavinkurve, N. Suryaprakash, ^{13}C–^{1}H HSQC experiment of probe molecules aligned in thermotropic liquid crystals: sensitivity and resolution enhancement in the indirect dimension, J. Magn. Reson. 185 (2007) 221–229.
[33] T.J. Norwood, Multiple quantum NMR methods, Prog. NMR Spectrosc. 24 (1992) 295–375.